Bubble Size Prediction for Rigid and Flexible Spargers

Nicholas W. Geary and Richard G. Rice
Dept. of Chemical Engineering, Louisiana State University, Baton Rouge, LA 70803

There exists a narrow operating window in bubble columns where the motion is so gentle that the normally dominating forces of coalescence and breakup no longer define the bubble size, hence formation dynamics must control. Elementary force balances are presented to predict bubble size, which compares favorably with experimental data and is shown to be applicable to both rigid and flexible spargers. The main focus is on the prediction and performance of a small-holed flexisparger, for which it is proved that the gas momentum term is highly significant. Also, it is shown that the intermediate drag law is more appropriate than Stokes for forming bubbles.

Introduction

Increasingly, it is the bubble size that is thought to be key in predicting tall bubble column dynamics. Recently, Rice and Geary (1990) proposed bubble diameter as the primary turbulence length scale to predict liquid circulation. This new theory compared favorably with a variety of experimental data. Earlier, Rice and Littlefield (1987) gave experimental evidence that the bubble diameter, not the column diameter, is the proper turbulence length scale for predicting axial dispersion in the bubbly regime.

Prince and Blanch (1990) recently argued that bubble size is controlled by a balance between the forces of coalescence and breakup. This, however, may not always be the case. For instance, it is well known that trace surfactants and salts reduce coalescence. Moreover, the stresses necessary for breakup to occur are insignificant when the turbulence Reynolds number $\leq 1{,}500$ (Stewart and Townsend, 1951). This limit is calculated directly from Kolmogoroff's theory of isotropic turbulence (e.g., Hinze, 1975), which makes use of the turbulent velocity as defined by Kawase and Moo-Young (1990). Bhavaraju et al. (1978) reported that bubble breakup does not occur in high-viscosity liquids even when the Reynolds number at the sparger hole exceeds 2,000. Thus, in systems where coalescence rates are insignificant and the liquid motion is inadequate to break bubbles, it is clear that the bubble formation process must obviously control size distribution. Such low-stress environments are particularly attractive for bioprocessing operations, where large interfacial areas are needed but cell damage must be minimal.

The use of a force balance to determine formation bubble size is by no means original to this work, having been discussed at length in the review paper by Kumar and Kuloor (1970), following the pioneering work of Davidson and coworkers (Davidson and Schuler, 1966; Davidson and Harrison, 1963). It should be noted, however, that several operating regimes exist for bubble formation. For high gas flow applications, jetting is known to occur at fixed orifices. A plume of gas extends above the sparger with subsequent bubble formation occurring in a random process. Under such conditions, the notion of slow bubble growth (followed by detachment) from the sparger has no meaning. The flexisparger mitigates against such jetting phenomenon. At somewhat lower velocities, the bubble size formed can be predicted by an inertia-bouyancy balance such as the point source model developed by Davidson and Harrison (1963). Under such conditions, the influence of sparger type and size is practically negligible (Kumar and Kuloor, 1970), since the contribution by surface tension is small.

At even lower gas flow rates, a careful consideration of all the pertinent forces, which act in and around the orifice, is required, including surface tension and gas momentum contributions. Moreover, in the case of flexible spargers (Rice and Howell, 1986), careful attention must be given to the estimation of hole size, which increases with applied gas pressure. Considering these points, we attempt to develop a rather general model to forecast bubble size, especially applicable to small-holed devices.

Correspondence concerning this article should be addressed to R. G. Rice.

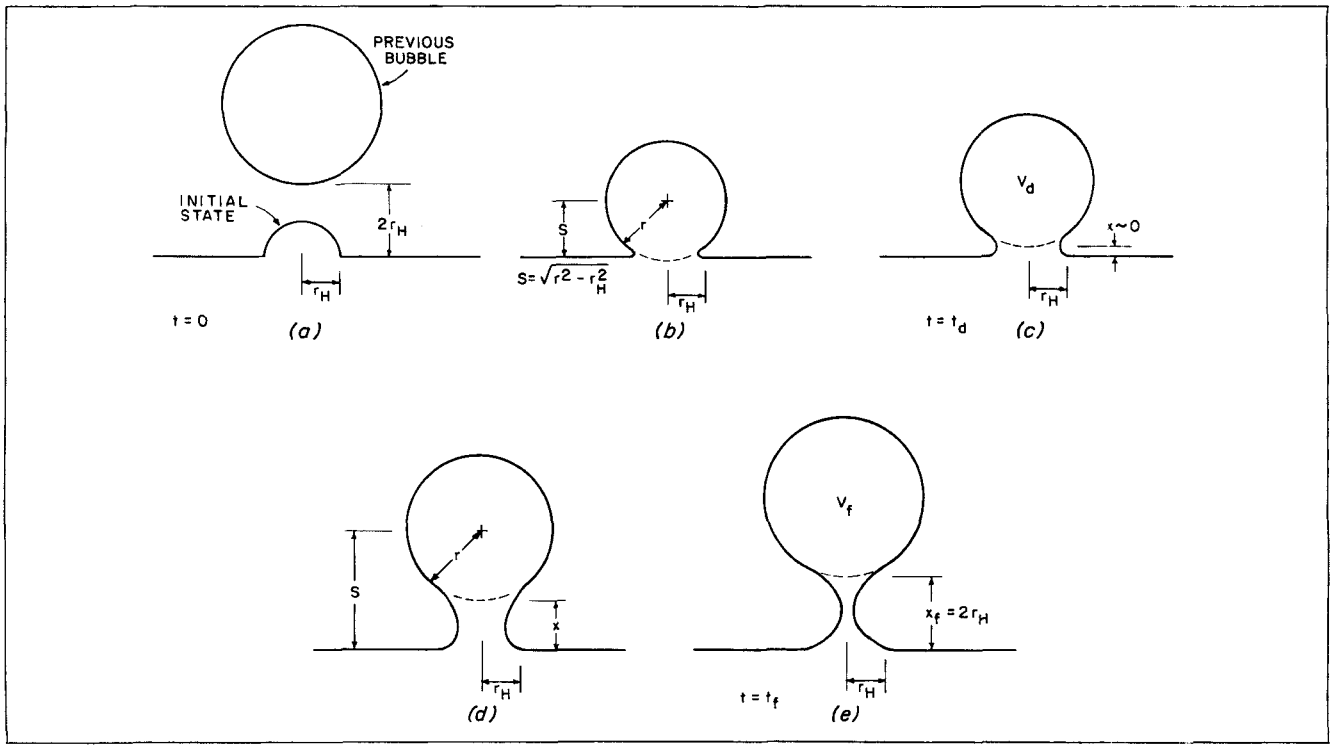

Figure 1. Bubble formation stages.

a. bubble birth, b. bubble expansion, c. bubble lift-off, d. bubble rise with continued expansion, and e. bubble detachment (final bubble size)

Theoretical Development

To begin the analysis, we consider first the curved interface formed within the interior of the orifice. This is the first stage of bubble birth, and we assume the interface has a radius equal to that of the orifice, Figure 1. This assumption is supported by experimental observations and agrees with the findings of Pincezewski (1981), LaNauze and Harris (1974), and Marmur and Rubin (1976). The formed bubble then grows until a force imbalance occurs, at which point the process of detachment can begin. The continually growing bubble then begins to rise vertically until the lens or neck, attaching it to the sparger, breaks. This point of final detachment, which has been the subject of debate, will be taken to occur when the bubble base is at a distance of twice the hole radius ($2r_H$) from the sparger surface. To support this, the very fundamental analysis of Kupferberg and Jameson (1969) suggested that the detachment height occurs between r_H and $2r_H$, while Pinczewski (1981) experimentally observed that the detachment occurred at approximately $2r_H$ (under practical conditions). Following Kupferberg and Jameson (1969), it could be argued that this process could occur first at $x_f = r_H$, requiring the rupture to occur at the base of the preceding bubble. The difference the above modification would make is shown (cf. Figure 2) to be small, but the arguments concerning the precise conditions required for detachment (Rice and Howell, 1987) will probably continue.

The analysis now focuses on the force balance of a forming bubble. The modifications introduced here include the following. First, a gas flow momentum term is added, which we show is especially significant at higher gas hole velocities, such as in small-holed spargers. At even higher velocities, jetting occurs, but formation no longer occurs at the hole, as mentioned earlier. LaNauze and Harris (1974) and later Pinczewski (1981) also included the gas flow momentum to account for high gas density effects. Second, the drag coefficient, normally taken to be Stokesian, will be written as $10/\sqrt{Re}$ (after Kunii and Levenspiel, 1969), which corresponds more closely to the formation Reynolds number. Thus we can write the force balance on a forming bubble as (where $\rho_g << \rho_L$):

$$\underset{\text{buoyancy}}{V\rho_L g} + \underset{\substack{\text{gas}\\ \text{momentum}}}{\frac{G^2\rho_g}{\pi r_H^2}} - \underset{\substack{\text{surface}\\ \text{tension}}}{2\pi\sigma r_H\cos\theta} - \underset{\text{drag}}{F_D} = \underset{\text{inertia}}{\frac{d}{dt}(\alpha\rho_L V U_b)} \tag{1}$$

The drag force, F_D, defined as

$$F_D = 1/2 A_b \rho_L C_D U_b^2 \tag{2}$$

depends on the drag coefficient, C_D, which is a function of the bubble Reynolds number. Under practical conditions, we stipulate the following drag relations:

$$Re < 1 \qquad F_D = 6\pi\mu r U_b \tag{3}$$

$$1 \le Re \le 500 \qquad F_D = 5\pi\sqrt{\frac{\rho_L\mu}{2}}(rU_b)^{3/2} \tag{4}$$

where $r(t)$ denotes the instantaneous forming bubble radius.

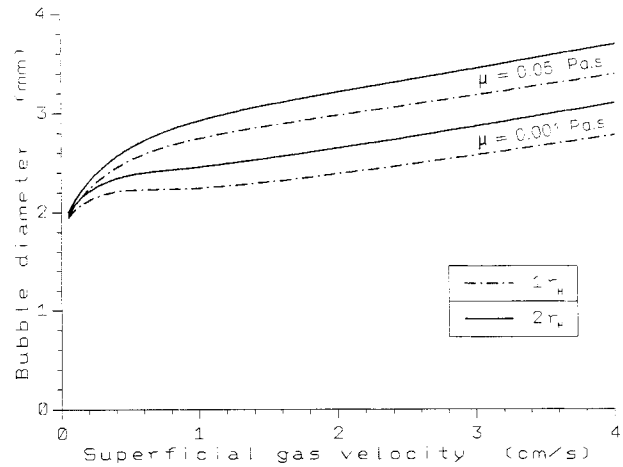

Figure 2. Comparison of two possible detachment criteria.

$x_f = r_H$ and $x_f = 2r_H$; physical conditions correspond to Figure 7.

Under the usual circumstance of constant gas flow, the bubble velocity, U_b, is determined using first the material balance:

$$\frac{dV}{d} = G \quad \text{or} \quad V = V_o + Gt \tag{5}$$

where the initial state is taken to be V_o at $t = 0$. This can also be written for an assumed spherical shape:

$$\frac{dV}{dt} = 4\pi r^2 \frac{dr}{dt} = G \tag{6}$$

In the earlier formation stage, we define (see Figure 1) bubble velocity:

$$U_b = \frac{dr}{dt} = \frac{G}{4\pi r^2} \tag{7}$$

hence from Eq. 7:

$$\frac{dU_b}{dt} = \frac{d}{dt}\left(\frac{G}{4\pi r^2}\right) = \frac{-2G^2}{(4\pi)^2 r^5} \tag{8}$$

For the typical conditions associated with forming bubbles ($Re \sim 100$) the force balance now becomes for the growth stage, taking $\cos\theta \simeq 1$ for aqueous systems:

$$\frac{4\pi}{3}\rho_L g r^3 + \frac{G^2\rho_g}{\pi r_H^2} - 2\pi\sigma r_H - 5\pi\sqrt{\frac{\rho_L\mu}{2}}\left(\frac{G}{4\pi r}\right)^{3/2} = \frac{\alpha\rho_L G^2}{12\pi r^2} \tag{9}$$

This dynamic balance is valid until an imbalance occurs at lift-off.

The value of α, the coefficient of virtual mass, will be taken to be 11/16. In previous studies (Davidson and Harrison, 1963; Rice and Howell, 1987), this coefficient was set equal to 1/2. Lamb (1932) originally derived the virtual mass coefficient for the equivalent case of a sphere accelerating away from a wall (see Figure 1d) as

$$\alpha = \frac{1}{2}\left(1 + \frac{3}{8}\frac{r^3}{s^3}\right) \tag{10}$$

where s is the distance from the center of the sphere to the wall. If, as is assumed here, the total distance traveled before detachment is $r_f + 2r_H$ and $r_H << r_f$, then s approximates to r, and thus α becomes 11/16 in the limit. The approximate model is useful, especially for small-holed spargers. Also, for very small holes, the assumption of sphericity seems warranted, since the small pucker illustrated in Figure 1 (not to scale) takes up a very small fraction of bubble surface area.

At some point, the growing bubble begins to lift off. At this point in time, Eq. 9 sustains an imbalance. We denote this time as t_d, the end of the growth period, and the corresponding radius is r_d. In the second stage, the bubble rises away from the sparger (and of course, continues to expand) until the attaching neck breaks. The governing equation for this stage is again described by a force balance of the type given above with the following modifications.

- The appropriate bubble velocity to be used is now a combination of bubble rise (away from the sparger surface, dx/dt) and bubble expansion (dr/dt), thus

$$U_b = dx/dt + dr/dt, \tag{11}$$

This modification is significant particularly in the acceleration term.

- To simplify the analysis, the appropriate velocity for the drag term will be taken as dr/dt. The error resulting from the omission of the dx/dt component is expected to be small in the drag term because the distance x_f is much less than the incremental bubble expansion ($r_f - r_d$). The acceleration term arising from the derivative of added lift velocity (dx/dt) is quite significant, however, and is accounted for in the inertia term.
- The neck or lens is modeled as a cylindrical column of length $x(t)$ and radius r_H; the actual shape of this neck is more along the lines shown in Figures 1d and 1e.

The balance for the second lift-off stage, where x denotes distance from the base of a bubble to the sparger surface, is thus taken to be:

$$\frac{4\pi}{3}\rho_L g r^3(T) + \frac{G^2\rho_g}{\pi r_H^2} - 2\pi\sigma r_H - 5\pi\sqrt{\frac{\rho_L\mu}{2}}\left[\frac{G}{4\pi r(T)}\right]^{3/2} - \frac{\alpha\rho_L G^2}{12\pi r^2(T)} = \alpha\rho_L \frac{d}{dT}\left[\frac{4\pi r^3(T)}{3}\frac{dx}{dx}\right] \tag{12}$$

where relative time T is defined as $T = t - t_d$, and t_f denotes the final time corresponding to bubble break-off [$x(T_f) = 2r_H$]. Bubble volume for the two stages are defined as:

$$V = V_d = \frac{4\pi}{3} r_d^3; \quad (t = t_d \quad \text{or} \quad T = 0) \tag{13}$$

$$V = V_d + GT = \frac{4\pi}{3} r^3(T); \quad (t_d < t < t_f) \tag{14}$$

and

$$V_f = V_d + GT_f = \frac{4\pi}{3} r_f^3; \ (t = t_f, \ T_f = t_f - t_d). \tag{15}$$

Applying the above substitutions to Eq. 12 gives the integrable result:

$$\frac{16g}{11}(V_d + GT) + F(r_H) - F(\mu)\frac{1}{\sqrt{V_d + GT}} - \frac{G^2}{12\pi}\left(\frac{4\pi}{3}\right)^{2/3}\left(\frac{1}{V_d + GT}\right)^{2/3} = \frac{d}{dT}\left(\frac{4\pi r^3}{3}\frac{dx}{dT}\right) \tag{16}$$

where the functions are defined as:

$$F(r_H) = \frac{16}{11\rho_L}\left(\frac{G^2\rho_g}{\pi r_H^2} - 2\pi\sigma r_H\right) \tag{16a}$$

$$F(\mu) = \left(\frac{8}{11}\right)5\pi\sqrt{\frac{2\mu}{\rho_L}}\left(\frac{G}{4\pi}\right)^{3/2}\left(\frac{4\pi}{3}\right)^{1/2} \tag{16b}$$

the first representing gas momentum of less retardation by surface tension and the second accounting for drag.

Integrating the above with the boundary condition $dx/dT = 0$ at $T = 0$, which describing initial lift-off velocity, produces the result:

$$\frac{16g}{11}\left(V_d T + \frac{1}{2}GT^2\right) + F(r_H) \times T - F(\mu)\left[\frac{2}{G}(\sqrt{V_d + GT} - \sqrt{V_d})\right] - G\left(\frac{1}{36\pi}\right)^{1/3} \times [(V_d + GT)^{1/3} - V_d^{1/3}] = \frac{4\pi r^3(T)}{3}\frac{dx}{dT} \tag{17}$$

Integrating the final state, by taking $x \cong 0$ at $T = 0$, results in:

$$\int_o^{2r_H} dx = \frac{8g(V_f - V_d)^2}{11G^2} - \frac{8g}{22G^2}[(V_f - V_d)(V_f - 3V_d) + 2V_d^2 \ln(V_f/V_d)] + F(r_H)\left[\frac{(V_f - V_d)}{G^2} - \frac{V_d}{G^2}\ln\left(\frac{V_f}{V_d}\right)\right] - \frac{4F(\mu)}{G^2}(V_f^{1/2} - V_d^{1/2}) + \frac{2F(\mu)}{G^2}\sqrt{V_d}\ln\left(\frac{V_f}{V_d}\right) - \left(\frac{3}{4\pi}\right)^{1/3}(V_f^{1/3} - V_d^{1/3}) + \left(\frac{1}{36\pi}\right)^{1/3} V_d^{1/3}\ln\left(\frac{V_f}{V_d}\right) \tag{18}$$

which can be written in dimensionless form:

$$2 = \frac{4gV_d^2}{11r_H G^2}[y^2 - 1 - 2\ln y] + N_r[y - 1 - \ln y] - N_\mu[2(y^{1/2} - 1) - \ln y] - \frac{V_d^{1/3}}{r_H}\left(\frac{1}{36\pi}\right)^{1/3}[3(y^{1/3} - 1) - \ln y] \tag{19}$$

where the following dimensionless groups arise:

$$N_r = \frac{16}{11}\frac{V_d}{\rho_L G^2 r_H}\left(\frac{G^2\rho_g}{\pi r_H^2} - 2\pi\sigma r_H\right) \tag{19a}$$

$$N_\mu = \frac{16}{11}\frac{5\pi\sqrt{V_d}}{r_H G^2}\sqrt{\frac{2\mu}{\rho_L}}\left(\frac{G}{4\pi}\right)^{3/2}\left(\frac{4\pi}{3}\right)^{1/2} \tag{19b}$$

and the ratio of final volume to expansion stage volume is:

$$y = \frac{V_f}{V_d}.$$

For low Reynolds numbers, drag is Stokesian, hence the third term on the righthand side may be replaced by

$$N_\mu^*\left[\frac{3}{2}(y^{2/3} - 1) - \ln y\right] \tag{20}$$

where

$$N_\mu^* = \frac{36}{11}\frac{V_d^{2/3}}{r_H G}\left(\frac{\mu}{\rho_L}\right)\left(\frac{4\pi}{3}\right)^{1/3} \tag{20a}$$

At this point, the theory is fully predictive and contains no adjustable parameters.

We next test the new theory using literature data. The selection of drag coefficient depends on the local Reynolds number and corresponds to the criterion given in Eqs. 3 and 4. Excellent agreement is obtained between the present theory and the fixed hole experimental data taken from Kumar and Kuloor (1970), as illustrated in Figure 3. A more direct comparison of the present theory with the data of Datta et al. (1950) and the model predictions by Kumar and Kuloor can be found in Table 1.

The agreement achieved thus far between the theory and some representative experimental data is quite good. However, a stronger test of the modifications introduced here will be undertaken by comparison with data taken from very-small-

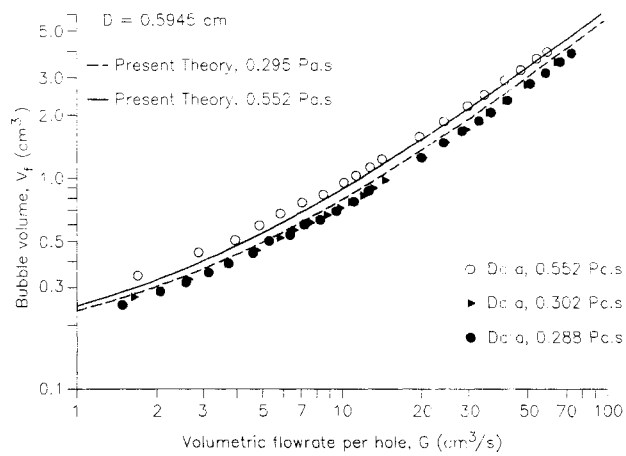

Figure 3. Test of present theory with data of Kumar and Kuloor (1970).

Table 1. Experimental Data of Datta et al. (1950) vs. Values Calculated from the General Model of Kumar and Kuloor (1970) and This Work

Physical Properties			D = 0.036 cm				D = 0.141 cm				D = 0.388 cm			
Viscosity μ Pa·s	Surface Tension σ 10^{-3}N/m	Density ρL g/cm^3	G, cm^3/s	Bubble Vol., cm^3			G, cm^3/s	Bubble Vol., cm^3			G, cm^3/s	Bubble Vol., cm^3		
				Experimental	Kumar & Kuloor	This Work		Experimental	Kumar & Kuloor	This Work		Experimental	Kumar & Kuloor	This Work
0.0012	72.8	0.9994	0.00810	0.0072	0.0107	0.0088	0.06083	0.0292	0.06114	0.0369	0.20500	0.0984	0.20723	0.1112
0.0154	68.3	1.1700	0.00787	0.0070	0.0077	0.0071	0.05208	0.0250	0.03188	0.0301	0.18120	0.0870	0.09653	0.0905
0.0255	67.6	1.1850	0.00787	0.0070	0.0077	0.0070	0.05104	0.0245	0.03121	0.0295	0.18120	0.0870	0.09137	0.0888
0.0497	66.4	1.2100	0.00765	0.0068	0.0075	0.0067	0.04812	0.0231	0.03114	0.0283	0.17170	0.0850	0.08762	0.0853
0.1108	65.7	1.2200	0.00765	0.0068	0.0074	0.0066	0.04583	0.0220	0.03006	0.0277	0.17500	0.0840	0.08645	0.0844

holed flexispargers. Before this can be done, the effect of (changing) initial hole size must be accounted for, and as noted earlier the flexisparger is self-regulating since holes expand and contract with increase or decrease in plenum chamber pressure.

Hole Size Calculation for Multiholed Flexispargers

The flexisparger is essentially a thin, elastic (usually rubber) membrane stretched over a hoop, with holes drilled or punctured in its face. Bubbles forming at these holes have been observed (Rice and Howell, 1987) to sustain excellent uniformity. In addition, it was noted that holes are self-regulating, increasing in size as the gas pressure rises. The analysis starts using the elastic mechanics developed by Rice and Howell (1987). They accounted for the elementary stress-strain relations in an expanding rubber sheet by way of a single extension ratio. This simplification arose by taking the membrane profile to be always spherical cap in shape.

They expressed the radius of curvature of an expanding, circular membrane to be:

$$R=\frac{Z^2+W_o^2}{2W_o} \tag{21}$$

where Z denotes hoop radius and W_o is the expanded centerline height, illustrated in Figure 4. By using the earlier work of Rivlin and Thomas (1951), who demonstrated that a circular hole in a rubber sheet expands according to

$$\frac{r_H}{r_{H_i}}=\lambda(r_s) \tag{22}$$

Rice and Howell (1987) deduced the elementary relationship for extension ratio:

$$\lambda=1+\frac{W(r_s)\,W_o}{Z^2} \tag{23}$$

This result is now modified to account for multiple holes at different radial positions (r_s) by introducing the concept of an average extension ratio, $\bar{\lambda}$, as simply

$$\bar{\lambda}=1+\frac{\overline{W}W_o}{Z^2} \tag{24}$$

where $\overline{W}$ is the average deflection height of the sparger defined as:

$$\overline{W}=\frac{1}{Z}\int_o^Z W(r_s)dr \tag{25}$$

Referring to Figure 4, it can be seen that $W(r_s)$ can be written as $W_o-R+\sqrt{R^2-r_s^2}$, which allows Eqs. 24 and 25 to be solved, yielding

$$\bar{\lambda}=1+\frac{W_o}{Z^2}\left\{(W_o-R)+\frac{1}{2Z}\left[Z\sqrt{R^2-Z^2}+R^2\sin^{-1}\left(\frac{Z}{R}\right)\right]\right\} \tag{26}$$

As pointed out by Rice and Howell (1987), the measurement of deflection at the center, W_o, allows $\bar{\lambda}$ to be calculated in a direct way from experimental measurements. Otherwise, the membrane shear modulus must be known (Rice and Howell, 1986) to estimate λ or $\bar{\lambda}$.

Now that the average extension ratio is known, it is easy to calculate hole size using Eq. 22, provided the initial (unexpanded) hole size, r_{H_i}, is known. To estimate this initial size, we use flow-pressure drop experiments along with the orifice equation:

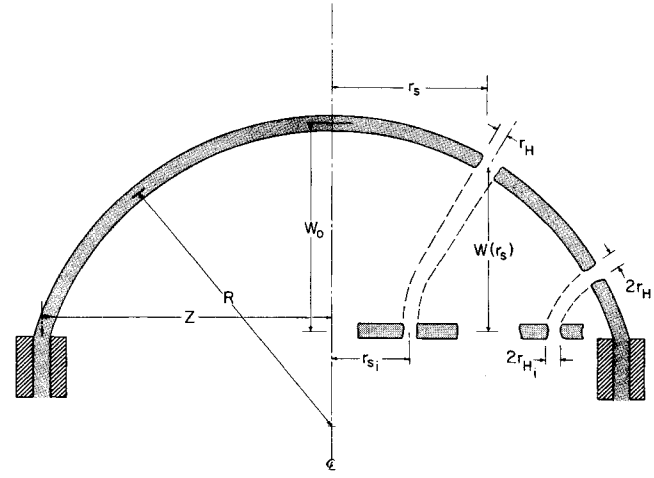

Figure 4. Expanded membrane showing dimensions and extension ratio definitions.

$$U_{og}A = N_H A_H C_o \sqrt{\frac{2}{\rho_g}\Delta p} \tag{27}$$

The pressure change (Δp) is computed from (Rice and Howell, 1987):

$$\Delta p = P_g - \rho_L g h \tag{28}$$

Assuming the discharge coefficient can be adequately represented by $C_o = K_o Re_h^n$ and that on average $\bar{r}_H = \bar{\lambda}\, r_{H_i}$, Eq. 27 becomes

$$\left(\frac{U_{og}A}{N_H}\right)^{(1-n)/(2-n)} (\Delta p)^{1/[2(n-2)]} = \bar{\lambda} r_{H_i} \left(\frac{K_o \pi^{1-n} \rho_g^{\,n-(1/2)} 2^{n+(1/2)}}{\mu_g^{\,n}}\right)^{1/(2-n)} \tag{29}$$

Elementary experiments on the sparger were undertaken which measured the sparger expansion height (W_o), pressure drop (Δp), and flow rate (U_{og}). The sparger used was 100 mm in diameter, had 110 holes, and was constructed from 3-mm-thick latex rubber sheet, stretched over a hollow cylinder. The results are plotted in the manner suggested by Eq. 29. The value of n was selected to match exactly the nonlinear parameter relationship. This requires the slope and the intercept in *Figure 5* to agree. The intercept of interest occurs when $\bar{\lambda} = 1$, thus the above optimization procedure can calculate only n. The second step is the determination of the coefficient K_o. An iterative routine was developed that fits this constant. The parameter search was constrained by the physical requirement that $0 < C_o < 1$. The value of K_o so estimated is then used to calculate the initial hole size. The final results from the parameter estimation routine are as follows.

K_o	n	$D_i(2r_{H_i})$ mm	Re_h	C_o
0.03	0.427	0.126	554–2,215	0.45–0.8

Thus, fluid flow/pressure drop measurements produced an average hole diameter of 0.126 mm.

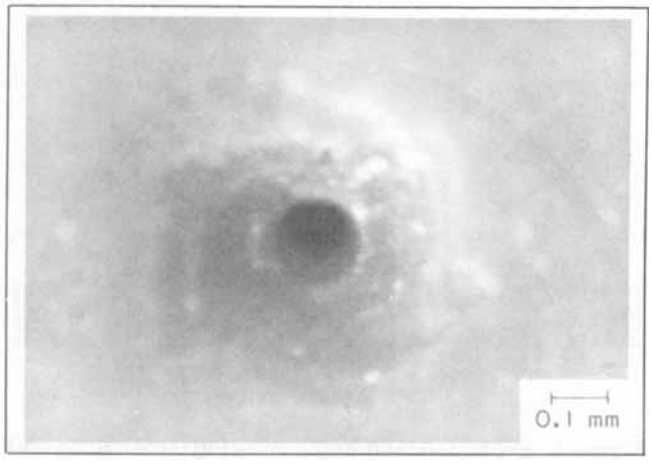

Figure 5. Unexpanded sparger hole.

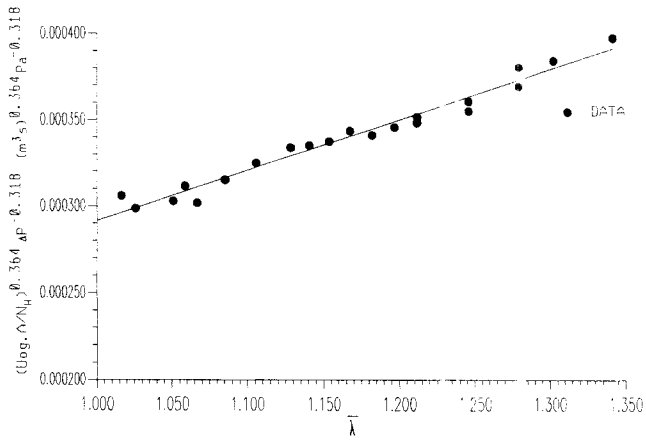

Figure 6. Test of Eq. 29 for linearity of extension ratio with view to determining the exponent in $C_o = K_o Re^n$.

Gradient = $2.92 \times 10^{-4} (m^3 \cdot s)^{0.364} (Pa)^{-0.318}$; $n = 0.427$

A final test of this implicit flow method is a comparison with the actual (photographed) hole diameter. To minimize measurement errors, the sparger was operated first to determine flow and pressure drop characteristics. It was then carefully removed and photographed, before being retested to be sure no changes (hysteresis) had occurred. The measurement technique used a ruled microscope slide (Spencer Hemacytometer, which is a ruled microscope slide used for making blood counts). The average hole diameter was found to be 0.138 mm (standard deviation was 0.02 mm, see Figure 5) by the photographic method. The value determined from the slope or intercept of the theory (Eq. 29) plotted in Figure 6 gave 0.126 mm, which agrees quite well with the photographic value.

The known values of $\bar{\lambda}$ and r_{H_i} allow the hole size r_H to be found from Eq. 22. This is then used in Eqs. 9 and 19 to yield the final prediction for bubble formation size (r_f). These computed results are given in Figure 7 along with the bubble size predicted by the Rice-Howell (1987) theory. We also illustrate the effect of ignoring gas momentum. The results apply to

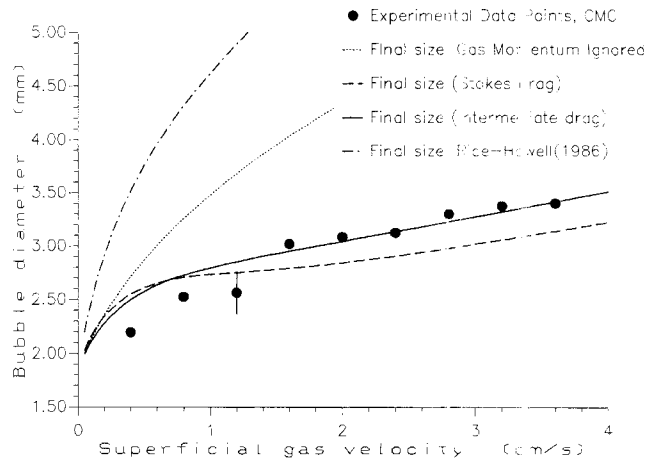

Figure 7. Influence of gas momentum and intermediate drag law on the present theory vs. experimental results for 0.025 Pa·s CMC solution.

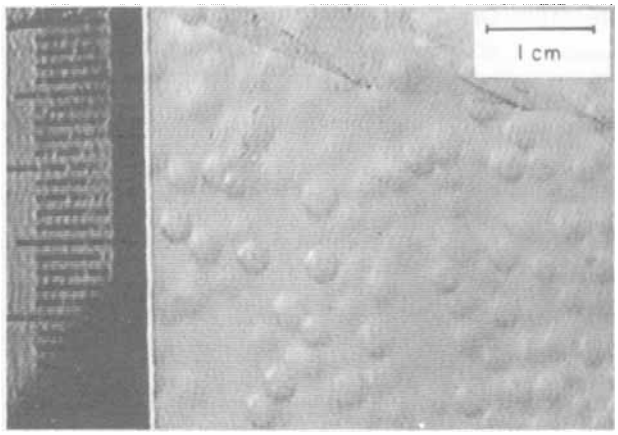

Figure 8. Image of bubbles within the bubble column, 0.05 Pa·s CMC.

oxygen bubbling in a 0.025 Pa·s CMC solution mounted within a 150-mm-diameter column. For such viscous solutions, Figure 7 also illustrates the difference in final bubble size if Stokes drag is used, rather than the intermediate law. The difference is small, but it is clear that the intermediate law seems to predict the data best. Experimental bubble size measurements, shown as points in Figure 7, are discussed next. Note in Table 1 and Figures 3 and 7 that all theoretical bubble size results are predictive and contain *no adjustable parameters*. We have also illustrated that bubble sizes are predictable for flexispargers provided the initial hole size (uninflated) is known. To design a flexisparger from first principles, the shear modulus of the elastic membrane must be known (Rice and Howell, 1986), along with membrane thickness.

A true test of the new bubble formation theory (which includes elastic mechanics) resides in comparison with measured bubble sizes. A physical technique was used, in which video tapes were made of the rising bubbles (Figure 8). The size of each bubble was determined by image analysis, in an initial clear liquid height of 2.2 meters. A reference grid placed in the column prior to experimentation supplied the necessary scaling information. For each successive flow rate, up to 80

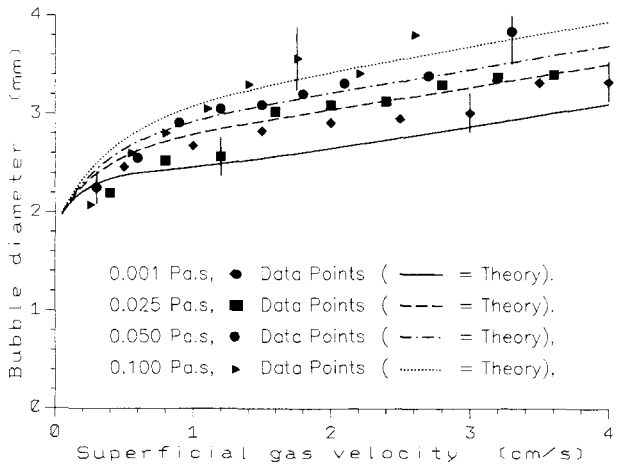

Figure 9. Present theory and experimental results for 0.001, 0.025, 0.05 and 0.1 Pa·s CMC.

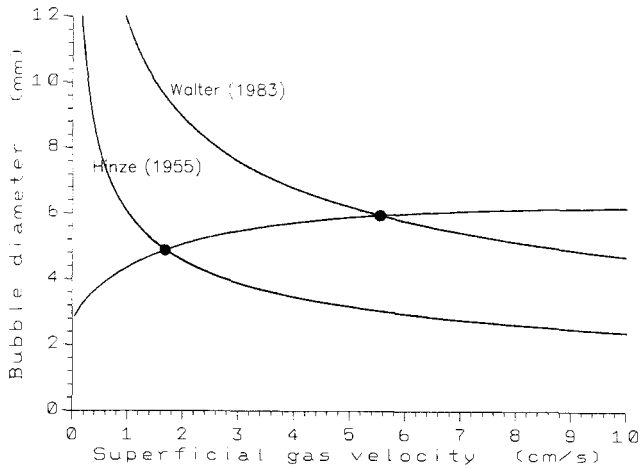

Figure 10. Bubble breakage limitation for Hills' column with 61 holes of 0.4 mm dia.

independent measurements were made for a total of four different viscosities (0.001, 0.025, 0.05 and 0.1 Pa·s CMC solutions). The results for the 0.025 Pa·s solution are plotted to be compared with the various theories given earlier. Figure 7 shows that good agreement between the present theory and experimental data is achieved. In addition, the use of an intermediate drag law seems warranted, especially at higher gas velocities, although the improvement over Stokes law is not as marked as the addition of the gas momentum term. The remaining experimental results are plotted in Figure 9, in which the points represent the average values and the error bars are calculated from the standard deviation. The new theory seems to give the correct viscosity dependence, especially for more viscous solutions. For very low gas velocities (10 mm/s), the effect of actual contact angle may be significant, since we have taken $\cos\theta \simeq 1$.

For practical applications, the upper range of the new theory is limited by the onset of breakage by turbulence forces, as discussed recently by Rice and Geary (1990). We illustrate this range in Figure 10 using the conditions corresponding to the aqueous bubble column reported by J. H. Hills (1974). Thus, as gas velocity increases, the present theory for bubble size intersects a size predicted for breakage. Two breakage curves are shown. The lowest curve shown is after the pioneering work of Hinze (1955) and the upper curve is a modification thereof by Walter (1983); these can be written, respectively:

$$d_b = 0.725(\sigma/\rho_L)^{0.6}/P_m^{0.4} \tag{30}$$

$$d_b = (\sigma/\rho_L)^{0.6}\left(\frac{\mu}{3\mu_g}\right)^{0.1}/P_m^{0.4} \tag{31}$$

where the energy dissipation per unit mass is taken to be $P_m \simeq U_{og}g$. The bold-faced point denotes possible transition points, above which formation dynamics no longer control. These critical points lie somewhere in the range $2 < U_{og} < 6$ cm/s, depending on the operative breakage curve.

Acknowledgment

We gratefully acknowledge support from the National Science Foundation, Grant No. CBT-8820472.

Notation

A = column cross-sectional area, cm^2
A_b = bubble cross-sectional area, cm^2
A_H = hole area, πr_H^2, cm^2
C_D = coefficient of drag
C_o = orifice coefficient
D = hole diameter, $2r_H$, cm
d_b = bubble size, cm
F_D = drag force, N
$F(r_H)$ = functions defined by Eq. 16a in force balance
$F(\mu)$ = functions defined by Eq. 16b in force balance
G = gas flow rate per hole, $cm^3 \cdot s^{-1}$
g = acceleration due to gravity, $cm \cdot s^{-2}$
h = height of clear liquid above the sparger, cm
K_o = multiplier in orifice coefficient equation
N_H = number of holes
N_r = dimensionless group defined by Eq. 19a
N_μ, N_μ^* = dimensionless group defined by Eq. 19b
P_g = gage pressure, Pa
P_m = energy dissipation per unit mass, cm^2/s^3
R = radius of curvature, sparger $(Z^2 + W_o^2)/2W_o$, cm
Re = bubble Reynolds number, $(2rU_b)/\nu = G/(2\pi r\nu)$
Re_h = hole Reynolds number, $2G/(\pi r_H \nu_g)$
r = radius of a bubble at time t, cm
r_d = bubble radius after stage 1, cm
r_f = bubble radius after stage 2, final size, cm
r_H = hole radius, cm
r_{H_i} = initial hole radius, no flow, cm
r_s = distance from the center of sparger to the hole, cm
r_{s_i} = original distance from center line of sparger to a hole with no expansion, initial position, cm
s = distance from bubble center to sparger face, cm
$T = t - t_d$, s
t = time, s
t_d = time to form stage-one bubble, s
t_f = final time to form stage two bubble, s
U_b = bubble rise velocity, cm/s
V = bubble volume at time t, cm^3
V_o = bubble volume at time $t = 0$, initial size, cm^3
V_d = bubble volume after stage one, cm^3
V_f = bubble volume after stage two, final size, cm^3
W_o = deflection of the pole, cm
$W(r_s)$ = deflection of membrane at position r_s, $[W(o) = W_o,\ W(Z) = 0]$, cm
x = distance from sparger surface to bubble base
x_f = distance from sparger to bubble base at detachment
$y = V_f/V_d$
Z = sparger radius, cm

Greek letters

α = virtual mass coefficient
δ = local microscale of turbulence
θ = surface tension contact angle, radians
$\underline{\lambda}$ = extension ratio
λ = average extension ratio
μ = liquid viscosity, Pa·s
μ_g = gas viscosity, Pa·s
ν = kinematic viscosity of the liquid, $cm^2 \cdot s^{-1}$
ρ_L = liquid density, $g \cdot cm^{-3}$
ρ_g = gas density, $g \cdot cm^{-3}$
σ = surface tension, $N \cdot m^{-1}$

Literature Cited

Bhavaraju, S. M., T. W. F. Russell, and H. W. Blanch, "The Design of Gas-Sparged Devices for Viscous Liquid Systems," *AIChE J.*, **24**, 454 (May, 1978).

Datta, R. L., D. H. Napier, and D. M. Newitt, "The Properties and Behaviour of Gas Bubbles Formed at a Circular Orifice," *Trans. Instn. Chem. Engrs.*, London, **28**, 14 (1950).

Davidson, J. F., and D. Harrison, *Fluidised Particles*, Cambridge University Press, 50 (1963).

Davidson, J. F., and B. O. G. Schuler, "Bubble Formation at an Orifice in a Viscous Liquid," *Trans. Instn. Chem. Engrs.*, **38**, 144 (1966).

Deckwer, W. D., A. Schumpe, K. Nguyen-Tien, and Y. Serpemen, "Oxygen Mass Transfer into Aerated C.M.C. Solutions in a Bubble Column," *Biotech. and Bioeng.*, **24**, 461 (1982).

Hinze, J. O., *Turbulence*, 2nd ed., McGraw-Hill, New York, 273 (1975).

Hinze, J. O., "Fundamentals of the Hydrodynamic Mechanism of Splitting in Dispersion Processes," *AIChE J.*, **1**, 289 (Sept., 1955).

Hills, J. H., "Radial Nonuniformity of Velocity and Voidage in a Bubble Column," *Trans. Instn. Chem. Eng.*, **52**, 1 (1974).

Kawase, Y., and M. Moo-Young, "Mathematical Models for Design of Bioreactors: Applications of Kolmogoroff's Theory of Isotropic Turbulence," *Chem. Eng. J.*, **43**, B19 (1990).

Kumar, R., and N. R. Kuloor, "The Formation of Bubbles and Drops," *Adv. in Chem. Eng.*, **8**, 255 (1970).

Kunii, D., and O. Levenspiel, *Fluidization Engineering*, Wiley, New York, 76 (1969).

Kupferberg, A., and G. J. Jameson, "Bubble Formation at a Submerged Orifice above a Gas Chamber of Infinite Volume," *Trans. Instn. Chem. Engrs.*, **47**, T241 (1969).

Lamb, H., *Hydrodynamics*, Dover Publications, 130 (1932).

LaNauze, R. D., and I. J. Harris, "Gas Bubble Formation at Elevated Pressures," *Trans. Instn. Chem. Engrs.*, **52**, 337 (1974).

Marmur, A., and E. Rubin, "A Theoretical Model for Bubble Formation at an Orifice Submerged in an Inviscial Liquid," *Chem. Eng. Sci.*, **11**, 453 (1976).

Pinczewski, W. V., "The Formation and Growth of Bubbles at a Submerged Orifice," *Chem. Eng. Sci.*, **36**, 405 (1981).

Prince, M. J., and H. W. Blanch, "Bubble Coalescence and Break-Up in Air-Sparged Bubble Columns," *AIChE J.*, **36**, 1485 (Oct., 1990).

Rice, R. G., D. T. Barbe, and N. W. Geary, "Correlation of Non-verticality and Entrance Effects in Bubble Columns," *AIChE J.*, **36**, 1421 (Sept., 1990).

Rice, R. G., and N. W. Geary, "Prediction of Liquid Circulation in Viscous Bubble Columns," *AIChE J.*, **36**, 1339 (Sept., 1990).

Rice, R. G., and S. W. Howell, "Bubble Formation from Elastic Holes," *Chem. Eng. Commun.*, **59**, 229 (1987).

Rice, R. G., and S. W. Howell, "Elastic and Flow Mechanics for Membrane Spargers," *AIChE J.*, **32**, 1377 (Aug., 1986).

Rivlin, R. S., and A. G. Thomas, "Large Elastic Deformations of Isotropic Materials: VIII. Strain Distribution around a Hole in a Sheet," *Philos. Trans. R. Soc.*, London, Ser. A, **243**, 289 (1951).

Stewart, R. W., and A. A. Townsend, "Similarity and Self-Preservation in Isotropic Turbulence," *Philos. Trans. R. Soc.*, London, Ser. A, **243**, 359 (1951).

Walter, J. W., "Bubble Breakup and Mass Transfer in Gas-Liquid Contactors," PhD Thesis, Univ. of California, Berkeley (1983).

Manuscript received Aug. 21, 1990, and revision received Nov. 19, 1990.